Liquid-Phase Exfoliation of Graphite into Single- and Few-Layer Graphene with α-Functionalized Alkanes

Sébastien Haar,[†] Matteo Bruna,[§] Jian Xiang Lian,[‡] Flavia Tomarchio,[§] Yoann Olivier,[*,‡] Raffaello Mazzaro,[∥,∆] Vittorio Morandi,[∥] Joseph Moran,[†] Andrea C. Ferrari,[§] David Beljonne,[‡] Artur Ciesielski,[†] and Paolo Samorì[*,†]

[†]Institut de Science et d'Ingénierie Supramoléculaires (ISIS) and International Center for Frontier Research in Chemistry (icFRC), Université de Strasbourg and Centre National de la Recherche Scientifique (CNRS), 8 alleé Gaspard Monge, 67000 Strasbourg, France

[§]Cambridge Graphene Centre, University of Cambridge, 9 JJ Thomson Avenue, Cambridge CB3 0FA, United Kingdom
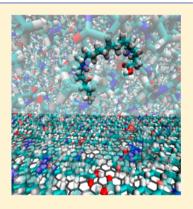
[‡]Laboratory for Chemistry of Novel Materials, Center for Research in Molecular Electronics and Photonics, University of Mons, Place du Parc 20, 7000 Mons, Belgium

[∥]Consiglio Nazionale delle Ricerche (CNR), Istituto per la Microelettronica e i Microsistemi (IMM) Sede di Bologna, Via Gobetti 101, 40129 Bologna, Italy

[∆]Dipartimento di Chimica "G. Ciamician", Università di Bologna, Via Selmi 2, 40126 Bologna, Italy

S *Supporting Information*

ABSTRACT: Graphene has unique physical and chemical properties, making it appealing for a number of applications in optoelectronics, sensing, photonics, composites, and smart coatings, just to cite a few. These require the development of production processes that are inexpensive and up-scalable. These criteria are met in liquid-phase exfoliation (LPE), a technique that can be enhanced when specific organic molecules are used. Here we report the exfoliation of graphite in *N*-methyl-2-pyrrolidinone, in the presence of heneicosane linear alkanes terminated with different head groups. These molecules act as stabilizing agents during exfoliation. The efficiency of the exfoliation in terms of the concentration of exfoliated single- and few-layer graphene flakes depends on the functional head group determining the strength of the molecular dimerization through dipole−dipole interactions. A thermodynamic analysis is carried out to interpret the impact of the termination group of the alkyl chain on the exfoliation yield. This combines molecular dynamics and molecular mechanics to rationalize the role of functionalized alkanes in the dispersion and stabilization process, which is ultimately attributed to a synergistic effect of the interactions between the molecules, graphene, and the solvent.

Graphene has unique physical and chemical properties including high charge mobility and current density, outstanding mechanical properties, optical transmittance, and thermal conductivity,[1] making it promising for various applications, for example, in electronics,[2] composites,[3−7] sensing,[8,9] and biomedicine.[10] Although several production methods have been proposed so far,[1,11] only a few among them are scalable and applicable at the industrial scale.[1,11] Liquid-phase exfoliation (LPE) of graphite enables the production of graphene in different solvents.[12−15] Typically, graphite can be exfoliated into single- and few-layer graphene (SLG and FLG, respectively) in a solvent having a surface tension (γ) close to 40 mJ m^{-2},[12,13,15] which favors an increase in the total area of graphite crystallites.[14] Therefore, solvents like *N*-methyl-2-pyrrolidone (NMP),[14] *ortho*-dichlorobenzene,[5,16] dimethylformamide,[17] and a few others[15] are commonly chosen as a dispersion media.[13] When subjected to sonication, graphite flakes split into individual graphene sheets that are stabilized in the liquid media.[18,19] During the ultrasound treatment, flakes of different size and thickness can be produced.[12] Centrifugation can then be used to separate SLG and FLG from unexfoliated material.[12,13,15]

To promote the exfoliation, organic molecules, in particular those having a high energy of adsorption on the graphene surface,[20−22] can be employed. In order to adsorb on the exfoliated graphene sheets, these dispersion-stabilizing agents (DSAs) need to have an adsorption energy higher than that of the solvent interacting with graphene.[20,22] In fact, the solvent dictates the choice of DSAs. Water, the "natural" solvent, has $\gamma \approx 72$ mJ m^{-2},[23] which is too high (≈ 30 mJ m^{-2} greater than NMP) for dispersing graphene and graphite.[24] However, by adding charged DSAs, such as pyrenes[25−28] or polymers,[29−33] exfoliation in water can be accomplished.[13,15] Nevertheless, water-based dispersions may not be suitable for all applications.

For example, water remaining at the interface with a dielectric substrate can result in charge-trapping, which is detrimental for application in electronics.[34] Therefore, DSA-assisted LPE in organic solvents is highly desirable. LPE of graphite in NMP can be assisted by the use of porphyrins,[35] lignin molecule derivatives,[31] salt derivatives,[36] and other systems.[15] However, a full understanding of the DSA role, needed for identifying the best DSAs to enhance the LPE process, is still lacking. References 20 and 22 reported that alkyl chains decorated with carboxylic acid groups can promote the exfoliation of graphene in NMP. Reference 22 also demonstrated that thermodynamics rules the self-assembly on graphene of fatty acids with different chain lengths, leading to an enhanced exfoliation when long aliphatic chains are used, as a result of a reduced translational and rotational entropic cost.[22]

Here we explore the impact of functional groups on the LPE Y_W (%), i.e., the yield of graphene exfoliation, defined as the ratio between the weight of dispersed graphitic material and that of the starting graphite flakes.[1,11] We show that the efficiency of the exfoliation in terms of Y_W and the quality of exfoliated flakes depends on the chemical nature of these groups. In particular, as DSA we employ a long linear $C_{21}H_{43}$ alkyl chain terminated with four chemical groups: (1) methyl (docosane), (2) alcohol (docosanol), (3) amine (docosan-1-amine), and (4) carboxylic acid (docosanoic acid) (see Figure 1). Combining molecular dynamics (MD) and statistical
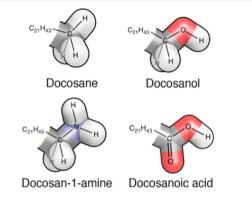

Figure 1. Schematic illustration of the $C_{21}H_{43}$ derivatives investigated in this paper.

mechanics, we discuss the thermodynamics of the graphene dispersion stabilization process. The most effective exfoliation is obtained with the aid of docosanoic acid (Y_W = 1.6%), with ~100% increase in Y_W when compared with that of the samples prepared upon exfoliation in pure NMP. While Y_W of LPE in the presence of docosane is 1.35%, docosanol and docosan-1-amine have lower performance (1 and 1.1%, respectively).

To achieve a full understanding of the effect of α-functionalization of the $C_{21}H_{43}$ alkyl chain on the molecular self-assembly on graphite/graphene, we perform a scanning tunneling microscopy (STM) study of physisorbed monolayers at the solid/liquid interface. This study is done by applying 4 μL of a 20 mM solution in 1-phenyloctane of the chosen $C_{21}H_{43}$ derivative onto freshly cleaved highly oriented pyrolitic graphite (HOPG). All of the molecules are found to lay flat on the HOPG surface and form monomorphic two-dimensional (2d) crystals, stable over several hours and extending over hundreds of nm^2. For the crystalline patterns obtained from each $C_{21}H_{43}$ derivative on HOPG, the unit cell parameters, that is, the length of the vectors a and b, α (the angle between the vectors), the unit cell area (A_{uc}), the number of molecules in the unit cell (n_{uc}), and the area occupied by a single molecule in the unit cell (A_{mol}), are reported in Table 1.

Figure 2a shows an STM image of the monolayer obtained from docosane, revealing a monocrystalline lamellar architecture. In this 2d assembly, docosane molecules are oriented perpendicular to the main lamellar axis. The supramolecular motif is stabilized both by molecule−molecule interaction at the intra- and interlamella levels as well as by molecule−substrate van der Waals interactions. A similar packing motif is observed for docosan-1-amine (Figure 2c). Notably, docosan-1-amine molecules are self-assembled in head-to-tail fashion between neighboring lamellas, a behavior that could not be observed for docosane due to its symmetric structure. The self-assembled structure of docosanoic acid is shown in Figure 2e. Docosanoic acid molecules form H-bonded dimers at the interlamellar level, with a molecular interdigitation between adjacent lamellae and the molecules oriented perpendicular to the main lamellar axis. Figure 2g portrays the STM image for a docosanol monolayer. Similarly to the docosanoic acid monolayers, docosanol molecules form H-bonded dimers. The geometry of the H-bonding between OH groups belonging to adjacent lamellae determines the ±60° angle between the molecule and lamella main axis. Furthermore, no interdigitation between molecules is observed

The unit cell parameters in Table 1 are in good agreement with earlier reports.[37−39] Given that the solvent used for STM experiments has to be apolar (dielectric constant $\varepsilon < 4$), the NMP solvent (ε = 31) employed for LPE cannot be used as a solvent to perform STM experiments at the solid/liquid interface.[40,41]

To test the influence of alkyl chain α-functionalization on Y_W and on the quality of exfoliated material, vials containing NMP, graphite powder, and the four DSAs, i.e., the different $C_{21}H_{43}$ derivatives, are exposed to bath sonication for 6 h (see the Experimental Section). Considering the area of the graphite/graphene surface occupied by a single $C_{21}H_{43}$ derivative (as determined from the unit cells in the STM images), the number

Table 1. Unit Cell Parameters of Monolayers of the $C_{21}H_{43}$ Derivatives Investigated in This Paper at the Solid/Liquid Interface[A]

$C_{21}H_{43}$ derivative	chemical formula	a (nm)	b (nm)	A (deg)	A_{uc} (nm²)	n_{uc}	A_{mol}
CH₃	$C_{21}H_{43}$−CH₃	0.4 ± 0.1	3.1 ± 0.1	(90 ± 2)	1.2 ± 0.2	1	1.2 ± 0.2
NH₂	$C_{21}H_{43}$−CH₂NH₂	0.4 ± 0.1	6.1 ± 0.1	(86 ± 2)	1.2 ± 0.2	1	1.2 ± 0.2
COOH	$C_{21}H_{43}$−COOH	0.9 ± 0.1	3.1 ± 0.1	(88 ± 2)	2.8 ± 0.2	2	1.4 ± 0.1
OH	$C_{21}H_{43}$−CH₂OH	0.4 ± 0.1	6.0 ± 0.1	(88 ± 2)	2.4 ± 0.2	2	1.2 ± 0.2

[A]a and b are the vector lengths and α the angle between those vectors; A_{uc} is the unit cell area, n_{uc} is the number of molecules in the unit cell, and A_{mol} (=A_{uc}/n_{uc}) is the area occupied by single molecules within the unit cell.
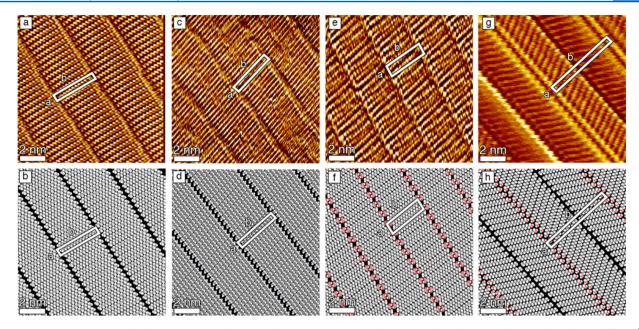
Figure 2. STM current images displaying monocrystalline lamellar architectures, as well as proposed molecular packing models, obtained from (a,b) docosane, (c,d) docosan-1-amine, (e,f) docosanoic acid, and (g,h) docosanol. Average tunneling current (I_t) = 20 pA; tip bias voltage (V_t) = 350 mV.

of molecules required to form densely packed monolayers is the number of molecules capable of covering 100% of the available ideal SLG surface area (s.a.).[20] Given that the real available SLG surface is much lower than the ideal one, because the exfoliated flakes are not only SLG but also multilayered,[12,14] we consider more realistic cases when an amount of molecules covering 2.5, 5, 7.5, 10, 15, and 20% of the ideal total available surface is used. Control samples consist of dispersions prepared in the absence of DSAs. After sonication and centrifugation, homogeneous dark dispersions are obtained and characterized by UV absorption spectroscopy (see Supporting Information, section S2). The presence of the molecules adsorbed on graphitic flakes can affect the mass measurements and, ultimately, Y_W. Thus, to quantify the concentration after centrifugation, a mixture of dispersion and chloroform is heated to 50 °C and filtered through polytetrafluoroethylene (PTFE) membranes. The remaining solvent and weakly interacting DSA molecules are washed out with copious amounts of diethyl ether and chloroform.[42] Measurements of the filtered mass are performed on a microbalance to infer the concentration.

By analyzing 10 control experiments, we find that when exfoliation is performed in the absence of DSAs, comparable Y_W values of dispersions (0.86%) are observed (Figure 3). Both Y_W
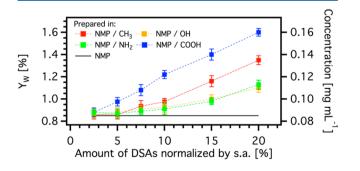
and the concentrations of dispersions produced through LPE in the presence of α-terminated $C_{21}H_{43}$ derivatives are reported in Figure 3. We find that in the presence of DSAs, Y_W increases almost linearly with an increasing amount of DSAs, regardless of α-functionalization.

Figure 3 reports the variation of Y_W as a function of the amount of DSA molecules expressed in s.a. %. The corresponding masses of DSA used in LPE are reported in Supporting Information, section S1. The most significant increase in Y_W is obtained by using 20% s.a. of docosanoic acid as DSAs, Y_W = 1.60%, and corresponds to a nearly 100% increase when compared to control samples. Also remarkable is the fact that the use of docosane as a DSA allows one to produce dispersions with $Y_W \approx 1.35\%$, outperforming the two remaining DSAs, i.e., docosanol and docosan-1-amine (1 and 1.1%, respectively). These results demonstrate the crucial choice of α-functionalization of aliphatic compounds acting as DSAs.

To provide a deeper understanding of the α-functionalization dependence on Y_W, we perform a thermodynamic analysis of DSAs/graphene interactions. The Y_W increase with the concentration of the DSAs in solution is associated with the formation of stable and spatially extended self-assembled monolayers (SAMs) physisorbed on the graphene surface. To understand the degree of stabilization of the liquid-phase exfoliated flakes with different DSAs, molecular dynamics/mechanics (MD/MM) calculations are used to analyze the thermodynamic properties of the self-assembled $C_{21}H_{43}$ derivative adlayers on graphene (Figure 1).

We employ the Groningen Machine for Chemical Simulations (Gromacs) 6.2 MD software[43−46] to simulate the ideal case of a SLG solvated in pure NMP using a package for building initial configurations for MD simulations (PACKMOL utility).[47] The SLG is frozen during the MD simulations. From the packing motifs observed in the STM experiments, solvated SAMs of docosane and its alcohol, amine, and acid derivatives on top of SLG are built (see Supporting Information, section S3). These structures are then simulated (see Supporting Information, section S3.1) after an initial optimization and

Figure 3. Variation of Y_W and concentration of flakes as a function of DSA molecules expressed in s.a. %. The error bars reflect a statistical analysis on 10 independent experiments.

equilibration of the systems. We discuss below the adsorption free energies and interaction energies extracted from these calculations, using in all cases the central molecule to avoid edge effects.

The entropic cost, the internal and free energy changes upon the adsorption of a single dispersion-stabilizing molecule on graphene, and its confinement in the SAM are reported in Figure 4a. The energies reported in Figure 4 do not take into
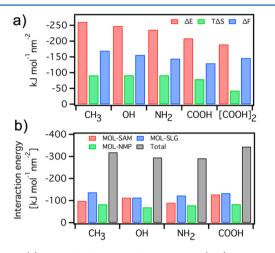

Figure 4. (a) Plot of the internal energy gain (ΔE), entropy cost ($T\Delta S$), and free energy difference (ΔF) per molecule per area for the DSA molecules in Figure 1, and for the docosanoic acid dimer [COOH]$_2$. (b) Decomposition of the total interaction energy per molecule and per surface area of DSA monomers with the SAM molecules, the graphene surface (SLG), and the NMP solvent.

account the work (PV) associated with a possible change in volume V at constant pressure P (negligible in the case of molecular adsorption on graphene) and correspond to Helmoltz free energies, where $\Delta F = \Delta E - T\Delta S$. The entropic contribution ($T\Delta S$) is calculated through a statistical mechanical approach assuming independent particles (i.e., ideal gas behavior) in the solvent phase (see Supporting Information, section S3.4). This approach was previously applied to describe the Y_W dependence with the chain length of carboxylic acids.[22] The change in internal energy per unit area upon bringing the molecule from the solvent to the graphene surface is largest for the bare alkane derivative, whereas the lowest energy gain is found for the docosanoic acid molecule. This is explained by the fact that the carboxylic acid strongly interacts with the polar NMP molecules (partly via hydrogen bonding), which tends to stabilize the acid in the solvent phase (naturally, these interactions are absent in the case of docosane). In the conditions considered here (T = 300 K, concentration of DSAs of 2 mM), the predicted entropy cost is very similar for all DSAs, as expected from their similar size (C22 derivatives).[22] Because the docosanoic acid has the largest unit cell (Table 1), the entropy change per unit area is reduced compared to that of other molecules. Altogether, the free energy change per molecule and per surface area for adsorption on graphene is mainly determined by the internal energy contribution.

Because the carboxylic acid molecules are known to dimerize through H-bonding[13,41,48] when the dimensionality is reduced from the three dimensions of a solution to the two dimensions on the graphene surface, we also compute the adsorption free energy of a docosanoic acid dimer. The internal energy per area

and per molecule is reduced (by ∼19 kJ mol^{-1} nm^{-2}) compared to that of a single acid molecule, while the entropy loss due to the confinement of the dimer in a 2d lattice is ∼86 kJ mol^{-1} nm^{-2} per dimer, i.e., ∼43 kJ mol^{-1} nm^{-2} per molecule, significantly smaller than that in the single-molecule case (∼79 kJ mol^{-1} nm^{-2}). Altogether, the change in free energy upon adsorption is more negative, indicating more favorable adsorption of the acid molecules in the dimer form. Yet, inspection of Figure 4a (see Supporting Information, Table S2) shows that, irrespective of whether we consider adsorption of monomers or dimers in the acid case, the trends in adsorption free energies do not match those in Y_W discussed above. In particular, the unfunctionalized alkane is predicted by theory to be the best DSA.

We thus consider another observable that better describes the affinity for the molecules to adsorb on graphene while simultaneously solubilizing the resulting graphene–organic hybrids: the total interaction energy between the central SAM molecule and its environment, i.e., the neighboring molecules in the SAMs, the solvent molecules (SOL), and the SLG surface. The calculations include all molecules within a cutoff radius of 1.3 nm from the probe central molecule, so as to reduce edge effects. As the molecules in Figure 1 present different packing geometries (see Supporting Information, Figures S3 and S4), the interaction energy per unit area is the relevant quantity because it considers the interactions of a single monomer with the surface and the solvent, as well as the degree of organization of the SAM at the surface.

Figure 4b portrays the different contributions to the interaction energies of the central monomer. The total interaction energy per molecule and per area is the largest in the case of the docosanoic acid. This arises mostly because of the formation of two H-bonds between the molecular head groups that strongly contribute to their largest interactions within the SAM (see MOL–SAM in Figure 4b). The unsubstituted docosane derivative displays the second highest total interaction energy per molecule and per area due to its largest interaction energy with the graphene surface (MOL–SLG, Figure 4b), promoted by the highest molecule density on graphene compared to that for other compounds (see Supporting Information, Table S3). The formation of the H-bonds between the docosanol molecules, in addition to the favorable chain–chain interactions, contributes to their stabilization within the SAM. However, the interaction energy with the SLG surface remains relatively small compared to that of the other C$_{21}$H$_{43}$ derivatives, due to the lower density of molecules on SLG. In the case of the amine derivative, the interactions with surrounding molecules in the SAM (MOL–SAM, Figure 4b) are weaker than those in the case of the alcohol derivative, likely due to a lower electronegativity of the nitrogen atom (compared to that of the oxygen of the alcohol group), resulting in a weaker H-bond between amine groups. Nevertheless, the MOL–SLG interaction is comparable to the docosanoic acid as the density of amine molecules on the SLG surface is similar to that of the acid. The interactions between the DSA and the NMP solvent (MOL–NMP, Figure 4b) are also comparable for all derivatives, and the hierarchy results from the different surface areas occupied by the molecules within the SAM (see Supporting Information, Table S3). Overall, the molecules bearing alcohol and amine functional groups have similar total interaction energies per molecule and per area and are lower than those of the alkane and acid derivatives. Thus, on the basis of the calculated interaction
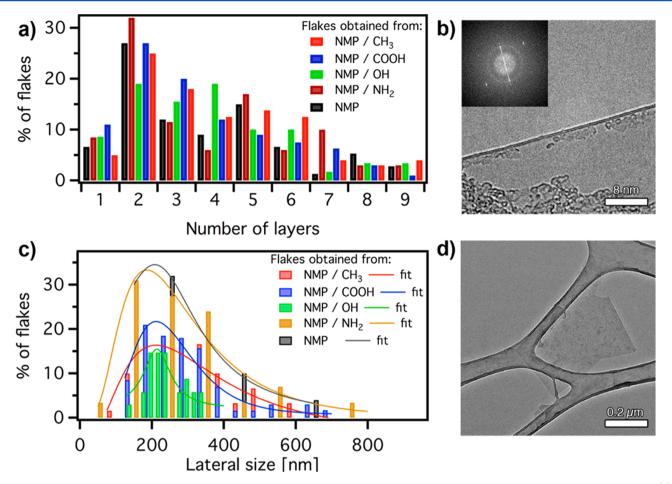
Figure 5. HR-TEM analysis of flakes exfoliated in NMP and in NMP with docosane, docosan-1-amine, docosanoic acid, and docosanol. (a) Distribution of the number of layers. (b) Micrograph of a representative BLG edge and fast Fourier transform (FFT), displaying the hexagonal pattern. (c) Flake size distribution; data fitted with a log normal function. (d) TEM micrograph of a representative SLG flake.

energies, the docosanoic acid is the most efficient DSA followed by the alkane and the alcohol/amine, in line with the experimental data.

High-resolution transmission electron microscopy (HR-TEM) is then used to gain quantitative information, such as the percentage of monolayers, the flake lateral size, as well as the presence/absence of defects. The analysis of the folded edges is used to estimate the number of layers.[49] We first consider the control sample, i.e., the dispersion prepared in the absence of DSAs. The TEM micrographs reveal a considerable fraction (~25%) of folded bilayer graphene (BLG) with lateral sizes < 0.8 μm, as usually observed for graphene produced via LPE.[12,13] We focus in particular on the dispersion exfoliated with 20 s.a.% DSAs as they give the highest increase of Y_W. In terms of lateral flake size, no major differences are monitored between the flakes exfoliated in NMP and those prepared in the presence of the different docosane derivatives, with a majority (~35%) of flakes having a size of 200 nm. The HR-TEM analysis shows that when DSA are used, the percentage of thinner flakes is higher compared to the case of the control sample. The statistical analyses of the number of layers and the flakes' lateral size are shown in Figure 5a,c.

Raman measurements are done on all samples to characterize the quality of the flakes. The dispersions are drop-cast on Si + 300 nm SiO$_2$ substrates, and the solvent is slowly evaporated on a hot plate at 100 °C. Raman spectra are acquired at 457, 514.5, and 633 nm with a Renishaw InVia with a 100× objective (N.A.

= 0.85). The power on the sample is kept below 1 mW to avoid any possible thermal damage. Thirty measurements are collected for the control dispersion in NMP as well as for those where docosanol, docosanoic acid, docosane, and docosan-1-amine are added. Figure 6 plots typical Raman spectra.

The G peak corresponds to the high-frequency E$_{2g}$ phonon at Γ.[50] The D peak is due to the breathing modes of six-atom rings and requires a defect for its activations.[49,51] It comes from transverse optical phonons around the Brillouin Zone (BZ) edge K, is active by double resonance, and is strongly dispersive with excitation energy due to a Kohn anomaly at K.[49,51] Double resonance can also happen as an intravalley process, i.e., connecting two points belonging to the same cone around K or K'. This gives the so-called D' peak. The 2D peak is the D peak overtone, and because it originates from a process where momentum conservation is satisfied by two phonons with opposite wave vectors, no defects are required for its activation.[52] The 2D peak is a single Lorentzian in SLG, whereas it splits into several components as the number of layers increases, reflecting the evolution of the electronic band structure.[49] In disordered carbons, the position of the G peak, Pos(G), increases with decreasing excitation wavelength (λ_L) from infrared to ultraviolet.[52] Therefore, the dispersion of the G peak, Disp(G), i.e., the rate of change of Pos(G) with the excitation wavelength, increases with disorder. The full width at half-maximum of the G peak, FWHM(G), also increases with
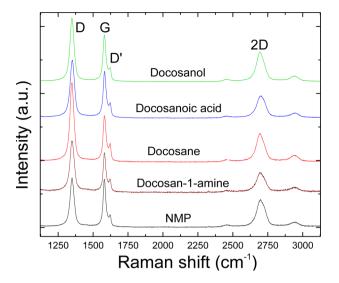
Figure 6. Raman spectra measured at 514.5 nm for flakes exfoliated in NMP and in the presence of $C_{21}H_{43}$ derivatives.

Figure 7. $I(D)/I(G)$ as a function of (a) FWHM(G), and (b) Disp(G) for control samples in NMP and samples produced in the presence of various DSAs. The error bars represent the spread of measured data.

disorder.[52] The analysis of the intensity ratio of the D and G peaks, $I(D)/I(G)$, combined with that of FWHM(G) and Disp(G) allows one to discriminate between disorder localized at the edges and in the bulk of the samples. In the latter case, a higher $I(D)/I(G)$ would correspond to higher FWHM(G) and Disp(G). Figure 7 indicates a correlation between these parameters. This implies that the treatment with docosanoic acid gives defects not localized just at the edges of the samples. Figure 7 also shows that CH_3 gives the least defective samples. Figure 7a shows that none of the representative spectra has a single Lorentzian line shape, consistent with the fact that the distribution of the number of layers is never centered on SLG, as for Figure 5a. Thus, even though COOH allows increasing Y_W, this happens at the expense of a higher number of defects, when compared to other $C_{21}H_{43}$ derivatives.

In conclusion, the use of α-functionalized alkanes as dispersion-stabilizing agents during LPE allows one to increase the yield of exfoliation by weight (Y_W) of graphite in liquid media. To understand the role of the functional group in α-substituted alkanes, we used the $C_{21}H_{43}$ alkyl chain as a scaffold and decorated it with simple, yet chemically distinctive groups, methyl, alcohol, amine, and carboxylic acid. The most effective exfoliation was obtained with docosanoic acid, with Y_W of 1.6%, with a ~100% increase in Y_W when compared to that of the control samples (0.8%). While Y_W of LPE carried out in the presence of docosane amounts to 1.35%, docosanol and docosan-1-amine have lower performance (1 and 1.1%, respectively). Our thermodynamic analysis suggests that aliphatic chains functionalized with carboxylic acid groups promote the stabilization of the exfoliated SLG and FLG in NMP due to synergistic interactions between the DSAs, the surface, and the polar solvent. The energy gain of a monomer upon adsorption on graphene prevails over the entropic cost of confinement in a 2d lattice, which is indistinguishable between different agents of the same size. The calculations based on a combination of MD and statistical mechanics allow for qualitative evaluation of the dispersion-stabilization efficiency and can be used to guide chemists toward the design of new DSAs for LPE.
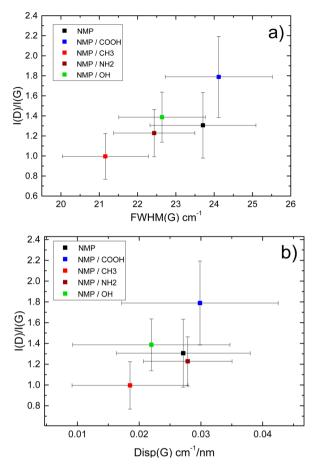
■ EXPERIMENTAL SECTION

N-Methyl-2-pyrrolidinone (product number (p.n.) 332461), graphite synthetic powder (p.n. 332461), docosanoic acid (p.n. 216941), docosanol (p.n. 169102), docosane (p.n. 43942), and 1-phenyloctane (p.n. 113190) were purchased from Sigma-Aldrich and used without any treatments.

Synthesis of Docosan-1-amine. The compound was prepared in 77% yield over three steps from 1-docosanol according to a modification of the procedure of refs 53 and 54 (see Supporting Information, section S1).

Scanning Tunneling Microscopy (STM). Analyses were carried out at the interface between a HOPG substrate and a supernatant solution by means of a Veeco multimode Nanoscope III. Solutions of a long linear alkane decorated with four different functions were applied to the basal plane of the surface. First, the substrates were glued to a magnetic disk, and an electric contact was made with silver paint (Aldrich Chemicals). Tips were mechanically cut from a Pt/Ir wire (90/10, diameter 0.25 mm). The raw STM data were processed through the application of background flattening, and the drift was corrected using the underlying graphite lattice as a reference. Before starting our measurements, the graphite lattice was visualized by lowering the bias voltage down to 20 mV and raising the current up to 65 pA. This allows confirmation of the good quality of the tip and the flatness of the substrate. A concentrated solution (2 M) of each molecule in Figure 1 was prepared in $CHCl_3$ and diluted with 1-

phenyloctane to provide solutions at a concentration of 20 mM. Solutions were heated overnight at 80 °C to completely dissolve the molecules. STM images were in constant height mode. To avoid tip crashes, the feedback loop was kept enabled. The formation of 2d patterns was attained by applying 3 μL of a solution onto freshly cleaved HOPG. The STM images were acquired at room temperature only after a negligible thermal drift was achieved.

Exfoliation of Graphite. Samples consisting of 1 wt % graphite powder in NMP were kept in a sonic bath for 6 h at 50 ± 2 °C (100 W). The temperature was kept constant to 50 °C by using a thermal controller and a cooling coil during sonication. To remove the large numbers of macroscopic aggregates of graphite, centrifugation (Eppendorf 5804, rotor F-34-6-38, 30 min at 10 000 rpm) was performed. Graphene dispersions (3 mL) were pipetted for each molecule, and a homogeneous dark phase was obtained. Additional experimental details are given in the Supporting Information, section S1.

Characterization. The amount of exfoliated flakes was measured on a Cubis Ultramicro-Balance MSA2.7S-000DM using a membrane holder. The filters were weighed five times before and after the filtration process in order to average the mass of graphene. Dispersions were transferred to a quartz cuvette (l = 10 mm) and analyzed by UV absorption spectroscopy using a Jasco V670 spectrophotometer equipped with a Peltier thermostated cell holder at 20 ± 0.05 °C. HR-TEM micrographs were taken on a FEI Tecnai F20 TEM equipped with a Schottky emitter and operated at 120 keV. The number of graphene layers was estimated from the number of (0,0,2) diffraction fringes at the edge of folded graphene sheets. The samples were prepared by drop-casting on a lacey carbon copper grid, followed by solvent evaporation at 150 °C for 10 min.

■ ASSOCIATED CONTENT

Ⓢ Supporting Information

The Supporting Information is available free of charge on the ACS Publications website at DOI: 10.1021/acs.jpclett.6b01260.

Liquid-phase exfoliation and molecular dynamics simulation details (PDF)

■ AUTHOR INFORMATION

Corresponding Authors

*(Y.O.) E-mail: yoann.olivier@umons.ac.be.
*(P.S.) E-mail: samori@unistra.fr.

Notes

The authors declare no competing financial interest.

■ ACKNOWLEDGMENTS

■ REFERENCES

(1) Ferrari, A. C.; Bonaccorso, F.; Fal'ko, V.; Novoselov, K. S.; Roche, S.; Boggild, P.; Borini, S.; Koppens, F. H. L.; Palermo, V.; Pugno, N.; et al. Science and Technology Roadmap for Graphene, Related Two-Dimensional Crystals, and Hybrid Systems. *Nanoscale* **2015**, *7*, 4598−4810.

(2) Westervelt, R. M. Applied Physics - Graphene Nanoelectronics. *Science* **2008**, *320*, 324−325.

(3) Lotya, M.; Hernandez, Y.; King, P. J.; Smith, R. J.; Nicolosi, V.; Karlsson, L. S.; Blighe, F. M.; De, S.; Wang, Z. M.; McGovern, I. T.; et al. Liquid Phase Production of Graphene by Exfoliation of Graphite in Surfactant/Water Solutions. *J. Am. Chem. Soc.* **2009**, *131*, 3611−3620.

(4) Torrisi, F.; Hasan, T.; Wu, W. P.; Sun, Z. P.; Lombardo, A.; Kulmala, T. S.; Hsieh, G. W.; Jung, S. J.; Bonaccorso, F.; Paul, P. J.; et al. Inkjet-Printed Graphene Electronics. *ACS Nano* **2012**, *6*, 2992−3006.

(5) El Gemayel, M.; Haar, S.; Liscio, F.; Schlierf, A.; Melinte, G.; Milita, S.; Ersen, O.; Ciesielski, A.; Palermo, V.; Samorì, P. Leveraging the Ambipolar Transport in Polymeric Field-Effect Transistors via Blending with Liquid-Phase Exfoliated Graphene. *Adv. Mater.* **2014**, *26*, 4814−4819.

(6) Boland, C. S.; Khan, U.; Backes, C.; O'Neill, A.; McCauley, J.; Duane, S.; Shanker, R.; Liu, Y.; Jurewicz, I.; Dalton, A. B.; et al. Sensitive, High-Strain, High-Rate Bodily Motion Sensors Based on Graphene-Rubber Composites. *ACS Nano* **2014**, *8*, 8819−8830.

(7) Mosciatti, T.; Haar, S.; Liscio, F.; Ciesielski, A.; Orgiu, E.; Samorì, P. A Multifunctional Polymer-Graphene Thin-Film Transistor with Tunable Transport Regimes. *ACS Nano* **2015**, *9*, 2357−2367.

(8) Schedin, F.; Geim, A. K.; Morozov, S. V.; Hill, E. W.; Blake, P.; Katsnelson, M. I.; Novoselov, K. S. Detection of Individual Gas Molecules Adsorbed on Graphene. *Nat. Mater.* **2007**, *6*, 652−655.

(9) Dua, V.; Surwade, S. P.; Ammu, S.; Agnihotra, S. R.; Jain, S.; Roberts, K. E.; Park, S.; Ruoff, R. S.; Manohar, S. K. All-Organic Vapor Sensor Using Inkjet-Printed Reduced Graphene Oxide. *Angew. Chem., Int. Ed.* **2010**, *49*, 2154−2157.

(10) Yang, W. R.; Ratinac, K. R.; Ringer, S. P.; Thordarson, P.; Gooding, J. J.; Braet, F. Carbon Nanomaterials in Biosensors: Should You Use Nanotubes or Graphene? *Angew. Chem., Int. Ed.* **2010**, *49*, 2114−2138.

(11) Bonaccorso, F.; Lombardo, A.; Hasan, T.; Sun, Z. P.; Colombo, L.; Ferrari, A. C. Production and Processing of Graphene and 2D Crystals. *Mater. Today* **2012**, *15*, 564−589.

(12) Coleman, J. N. Liquid Exfoliation of Defect-Free Graphene. *Acc. Chem. Res.* **2013**, *46*, 14−22.

(13) Ciesielski, A.; Samorì, P. Graphene via Sonication Assisted Liquid-Phase Exfoliation. *Chem. Soc. Rev.* **2014**, *43*, 381−398.

(14) Hernandez, Y.; Nicolosi, V.; Lotya, M.; Blighe, F. M.; Sun, Z. Y.; De, S.; McGovern, I. T.; Holland, B.; Byrne, M.; Gun'ko, Y. K.; et al. High-Yield Production of Graphene by Liquid-Phase Exfoliation of Graphite. *Nat. Nanotechnol.* **2008**, *3*, 563−568.

(15) Ciesielski, A.; Samorì, P. Supramolecular Approaches to Graphene: From Self-Assembly to Molecule Assisted Liquid-Phase Exfoliation. *Adv. Mater.* **2016**, DOI: 10.1002/adma.201505371.

(16) Hamilton, C. E.; Lomeda, J. R.; Sun, Z. Z.; Tour, J. M.; Barron, A. R. High-Yield Organic Dispersions of Unfunctionalized Graphene. *Nano Lett.* **2009**, *9*, 3460−3462.

(17) Li, X. L.; Zhang, G. Y.; Bai, X. D.; Sun, X. M.; Wang, X. R.; Wang, E.; Dai, H. J. Highly Conducting Graphene Sheets and Langmuir-Blodgett Films. *Nat. Nanotechnol.* **2008**, *3*, 538−542.

(18) Feng, R.; Zhao, Y. Y.; Zhu, C. P.; Mason, T. J. Enhancement of Ultrasonic Cavitation Yield by Multi-Frequency Sonication. *Ultrason. Sonochem.* **2002**, *9*, 231−236.

(19) Mason, T. J.; Lorimer, J. P. *Applied Sonichemistry.* Wiley-VCH Verlag: Weinheim, Germany, 2002.

(20) Ciesielski, A.; Haar, S.; El Gemayel, M.; Yang, H. F.; Clough, J.; Melinte, G.; Gobbi, M.; Orgiu, E.; Nardi, M. V.; Ligorio, G.; et al. Harnessing the Liquid-Phase Exfoliation of Graphene Using Aliphatic

Compounds: A Supramolecular Approach. *Angew. Chem., Int. Ed.* **2014**, *53*, 10355−10361.

(21) Conti, S.; del Rosso, M. G.; Ciesielski, A.; Weippert, J.; Böttcher, A.; Shin, Y. Y.; Melinte, G.; Ersen, O.; Casiraghi, C.; Feng, X. L.; et al. Perchlorination of Coronene Enhances its Propensity for Self-Assembly on Graphene. *ChemPhysChem* **2016**, *17*, 352−357.

(22) Haar, S.; Ciesielski, A.; Clough, J.; Yang, H. F.; Mazzaro, R.; Richard, F.; Conti, S.; Merstorf, N.; Cecchini, M.; Morandi, V.; et al. A Supramolecular Strategy to Leverage the Liquid-Phase Exfoliation of Graphene in the Presence of Surfactants: Unraveling the Role of the Length of Fatty Acids. *Small* **2015**, *11*, 1691−1702.

(23) Israelachvili, J. N. *Intermolecular and Surface Forces: Revised*, 3rd ed.; Academic Press: Oxford, U.K., 2011.

(24) Wang, S. R.; Zhang, Y.; Abidi, N.; Cabrales, L. Wettability and Surface Free Energy of Graphene Films. *Langmuir* **2009**, *25*, 11078−11081.

(25) Dong, X.; Shi, Y.; Zhao, Y.; Chen, D.; Ye, J.; Yao, Y.; Gao, F.; Ni, Z.; Yu, T.; Shen, Z.; et al. Symmetry Breaking of Graphene Monolayers by Molecular Decoration. *Phys. Rev. Lett.* **2009**, *102*, 135501.

(26) Parviz, D.; Das, S.; Ahmed, H. S. T.; Irin, F.; Bhattacharia, S.; Green, M. J. Dispersions of Non-Covalently Functionalized Graphene with Minimal Stabilizer. *ACS Nano* **2012**, *6*, 8857−8867.

(27) Schlierf, A.; Yang, H.; Gebremedhn, E.; Treossi, E.; Ortolani, L.; Chen, L.; Minoia, A.; Morandi, V.; Samorì, P.; Casiraghi, C.; et al. Nanoscale Insight into the Exfoliation Mechanism of Graphene with Organic Dyes: Effect of Charge, Dipole and Molecular Structure. *Nanoscale* **2013**, *5*, 4205−4216.

(28) Zhang, F.; Chen, X. J.; Boulos, R. A.; Yasin, F. M.; Lu, H. B.; Raston, C.; Zhang, H. B. Pyrene-Conjugated Hyaluronan Facilitated Exfoliation and Stabilisation of Low Dimensional Nanomaterials in Water. *Chem. Commun.* **2013**, *49*, 4845−4847.

(29) Guardia, L.; Fernandez-Merino, M. J.; Paredes, J. I.; Solis-Fernandez, P.; Villar-Rodil, S.; Martinez-Alonso, A.; Tascon, J. M. D. High-throughput Production of Pristine Graphene in an Aqueous Dispersion Assisted by Non-Ionic Surfactants. *Carbon* **2011**, *49*, 1653−1662.

(30) Liang, Y. T.; Hersam, M. C. Highly Concentrated Graphene Solutions via Polymer Enhanced Solvent Exfoliation and Iterative Solvent Exchange. *J. Am. Chem. Soc.* **2010**, *132*, 17661−17663.

(31) Liu, W. S.; Zhou, R.; Zhou, D.; Ding, G. G.; Soah, J. M.; Yue, C. Y.; Lu, X. H. Lignin-Assisted Direct Exfoliation of Graphite to Graphene in Aqueous Media and its Application in Polymer Composites. *Carbon* **2015**, *83*, 188−197.

(32) Popescu, M. T.; Tasis, D.; Tsitsilianis, C. Ionizable Star Copolymer-Assisted Graphene Phase Transfer between Immiscible Liquids: Organic Solvent/Water/Ionic Liquid. *ACS Macro Lett.* **2014**, *3*, 981−984.

(33) Uysal Unalan, I.; Wan, C. Y.; Trabattoni, S.; Piergiovanni, L.; Farris, S. Polysaccharide-Assisted Rapid Exfoliation of Graphite Platelets into High Quality Water-Dispersible Graphene Sheets. *RSC Adv.* **2015**, *5*, 26482−26490.

(34) Chua, L. L.; Zaumseil, J.; Chang, J. F.; Ou, E. C. W.; Ho, P. K. H.; Sirringhaus, H.; Friend, R. H. General Observation of n-Type Field-Effect Behaviour in Organic Semiconductors. *Nature* **2005**, *434*, 194−199.

(35) Malig, J.; Stephenson, A. W. I.; Wagner, P.; Wallace, G. G.; Officer, D. L.; Guldi, D. M. Direct Exfoliation of Graphite with a Porphyrin - Creating Functionalizable Nanographene Hybrids. *Chem. Commun.* **2012**, *48*, 8745−8747.

(36) Yeon, C.; Yun, S. J.; Lee, K. S.; Lim, J. W. High-Yield Graphene Exfoliation Using Sodium Dodecyl Sulfate Accompanied by Alcohols as Surface-Tension-Reducing Agents in Aqueous Solution. *Carbon* **2015**, *83*, 136−143.

(37) Giancarlo, L.; Cyr, D.; Muyskens, K.; Flynn, G. W. Scanning Tunneling Microscopy of Molecular Adsorbates at the Liquid-Solid interface: Functional Group Variations in Image Contrast. *Langmuir* **1998**, *14*, 1465−1471.

(38) Hibino, M.; Sumi, A.; Tsuchiya, H.; Hatta, I. Microscopic Origin of the Odd-Even Effect in Monolayer of Fatty Acids Formed on a Graphite Surface by Scanning Tunneling Microscopy. *J. Phys. Chem. B* **1998**, *102*, 4544−4547.

(39) Yang, T.; Berber, S.; Liu, J. F.; Miller, G. P.; Tomanek, D. Self-Assembly of Long Chain Alkanes and Their Derivatives on Graphite. *J. Chem. Phys.* **2008**, *128*, 124709.

(40) Ciesielski, A.; Samorì, P. Supramolecular Assembly/Reassembly Processes: Molecular Motors and Dynamers Operating at Surfaces. *Nanoscale* **2011**, *3*, 1397−1410.

(41) Ciesielski, A.; Palma, C.-A.; Bonini, M.; Samorì, P. Towards Supramolecular Engineering of Functional Nanomaterials: Pre-Programming Multi-Component 2D Self-Assembly at Solid-Liquid Interfaces. *Adv. Mater.* **2010**, *22*, 3506−3520.

(42) Döbbelin, M.; Ciesielski, A.; Haar, S.; Osella, S.; Bruna, M.; Minoia, A.; Grisanti, L.; Mosciatti, T.; Richard, F.; Prasetyanto, E. A.; et al. Light-Enhanced Liquid-Phase Exfoliation and Current Photoswitching in Graphene-Azobenzene Composites. *Nat. Commun.* **2016**, *7*, 11090.

(43) Berendsen, H. J. C.; Vanderspoel, D.; Vandrunen, R. Gromacs - a Message-Passing Parallel Molecular-Dynamics Implementation. *Comput. Phys. Commun.* **1995**, *91*, 43−56.

(44) Hess, B.; Kutzner, C.; van der Spoel, D.; Lindahl, E. GROMACS 4: Algorithms for Highly Efficient, Load-Balanced, and Scalable Molecular Simulation. *J. Chem. Theory Comput.* **2008**, *4*, 435−447.

(45) Lindahl, E.; Hess, B.; van der Spoel, D. GROMACS 3.0: a Package for Molecular Simulation and Trajectory Analysis. *J. Mol. Model.* **2001**, *7*, 306−317.

(46) Van der Spoel, D.; Lindahl, E.; Hess, B.; Groenhof, G.; Mark, A. E.; Berendsen, H. J. C. GROMACS: Fast, Flexible, and Free. *J. Comput. Chem.* **2005**, *26*, 1701−1718.

(47) Martinez, L.; Andrade, R.; Birgin, E. G.; Martinez, J. M. PACKMOL: A Package for Building Initial Configurations for Molecular Dynamics Simulations. *J. Comput. Chem.* **2009**, *30*, 2157−2164.

(48) Haar, S.; El Gemayel, M.; Shin, Y. Y.; Melinte, G.; Squillaci, M. A.; Ersen, O.; Casiraghi, C.; Ciesielski, A.; Samorì, P. Enhancing the Liquid-Phase Exfoliation of Graphene in Organic Solvents upon Addition of n-Octylbenzene. *Sci. Rep.* **2015**, *5*, 16684.

(49) Ferrari, A. C.; Meyer, J. C.; Scardaci, V.; Casiraghi, C.; Lazzeri, M.; Mauri, F.; Piscanec, S.; Jiang, D.; Novoselov, K. S.; Roth, S.; et al. Raman Spectrum of Graphene and Graphene Layers. *Phys. Rev. Lett.* **2006**, *97*, 187401.

(50) Tuinstra, F.; Koenig, J. L. Raman Spectrum of Graphite. *J. Chem. Phys.* **1970**, *53*, 1126−1130.

(51) Ferrari, A. C.; Robertson, J. Resonant Raman Spectroscopy of Disordered, Amorphous, and Diamondlike Carbon. *Phys. Rev. B: Condens. Matter Mater. Phys.* **2001**, *64*, 075414.

(52) Ferrari, A. C.; Basko, D. M. Raman Spectroscopy as a Versatile Tool for Studying the Properties of Graphene. *Nat. Nanotechnol.* **2013**, *8*, 235−246.

(53) Lin, W. Q.; Zhang, X. M.; He, Z.; Jin, Y.; Gong, L. Z.; Mi, A. Q. Reduction of Azides to Amines or Amides with Zinc and Ammonium Chloride as Reducing Agent. *Synth. Commun.* **2002**, *32*, 3279−3284.

(54) Sugandhi, E. W.; Macri, R. V.; Williams, A. A.; Kite, B. L.; Slebodnick, C.; Falkinham, J. O.; Esker, A. R.; Gandour, R. D. Synthesis, Critical Micelle Concentrations, and Antimycobacterial Properties of Homologous, Dendritic Amphiphiles. Probing Intrinsic Activity and the "Cutoff" Effect. *J. Med. Chem.* **2007**, *50*, 1645−1650.